GEOPHYSICAL RESEARCH LETTERS, VOL. 35, L22606, doi:10.1029/2008GL035152, 2008

Dynamic ocean topography for the northeast Pacific and its continental margins

M. G. G. Foreman,[1] W. R. Crawford,[1] J. Y. Cherniawsky,[1] and J. Galbraith[2]

Received 26 June 2008; revised 10 October 2008; accepted 16 October 2008; published 27 November 2008.

[1] Estimates of dynamic ocean (or sea surface) topography based on satellite altimetry and gravity observations generally become degraded as they approach land. In this study, dynamic ocean topography for the northeast Pacific Ocean is computed independently of satellite observations using a high resolution model and seasonal climatologies of temperature, salinity, and wind stress. Comparisons with estimates based on satellite gravity and altimetry measurements show reasonable agreement in the deep ocean but are poor on continental margins where the ocean model estimates not only reveal significant seasonal differences, but are also shown to be reasonably accurate when compared with satellite altimetry and coastal tide gauge measurements. The dynamic ocean topography estimates provided here will permit more accurate calculations of the geoid and satellite altimeter absolute heights and currents. **Citation:** Foreman, M. G. G., W. R. Crawford, J. Y. Cherniawsky, and J. Galbraith (2008), Dynamic ocean topography for the northeast Pacific and its continental margins, *Geophys. Res. Lett.*, *35*, L22606, doi:10.1029/2008GL035152.

1. Introduction

[2] Mean dynamic ocean topography (DOT) is the difference between a time-averaged sea surface and a geoid, and is directly related to the average (steady-state) surface currents. Horizontal gradients in DOT (sometimes referred to as sea surface topography) arise from a variety of factors that include sea surface wind stress, horizontal gradients in air pressure and in the vertical integral of water density, and tidal rectification. As seawater density is a function of temperature, salinity, and depth (pressure), density variations are largely due to temperature and salinity variations and these in turn arise from river runoff, precipitation, evaporation, ice melting and freezing, advection by currents, mixing, and atmospheric heating/cooling. As observations from the GRACE, CHAMP, TOPEX/Poseidon/Jason (TPJ), ERS1-2 and Envisat satellite missions continue to accumulate, global estimates of DOT have become available from the Jet Propulsion Laboratory (http://grace.jpl.nasa.gov) and AVISO (http://www.aviso.oceanobs.com/). The JPL product is computed purely from GRACE gravity measurements, while AVISO's Combined Mean Dynamic Topography (CMDT) product, Rio05 [*Rio and Hernandez*, 2004], is computed with a multi-variate analysis using seawater temperature and salinity data [*Boyer et al.*, 2002; *Stephens et al.*, 2002], ocean surface drifter velocities, and TPJ and ERS1-2 altimetry over the period 1993–99. Both products are available on a 0.5° resolution grid.

[3] Dynamic ocean topography can also be estimated by free-surface numerical ocean models that may or may not assimilate satellite altimetry and tide gauge observations. K. Thompson et al. (The mean sea surface topography of the North Atlantic: Comparison of estimates based on satellite, terrestrial gravity and oceanographic observations, submitted to *Journal of Geophysical Research*, 2008) estimated a mean surface topography for the North Atlantic Ocean by averaging model elevations over nine years and evaluated model accuracy by comparing its surface velocities with GRACE geostrophic currents and near-surface drifter observations. Using an ensemble of five models, *Bingham and Haines* [2006] computed a similar estimate of both the DOT and its root mean square errors. However the models in these studies were not of sufficiently high spatial resolution to capture the nearshore details that would permit a comparison with coastal tide gauge sea levels.

[4] Our modelling approach is somewhat different. Rather than averaging over one or more multi-year model simulations, we average multi-year observations of the features influencing dynamic ocean topography; namely temperature, salinity, and wind stress, and use these to force a diagnostic model whose irregular grid provides high spatial resolution of continental margins and coastal regions. Though the model calculation is analogous to conventional dynamic height calculations, it does not require a level of no motion and can include winds, frictional effects due to tides, and inflows along the open ocean boundaries.

2. The Model Calculation

[5] The model employed for our simulations is FUNDY5SP [*Greenberg et al.*, 1998], a spherical coordinate extension of the finite element code FUNDY5 developed by *Lynch and Werner* [1987]. The domain covers the region east of 160°W longitude and north of 30°N latitude and the triangular grid was constructed with the software package GRIDGEN and its predecessor TRIGRID [*Henry and Walters*, 1993]. It has 97,959 nodes, 169,869 triangles and a resolution that varies from 100 m in some narrow coastal channels to 70 km in the deep ocean. The grid is essentially a combination of that used by *Foreman et al.* [2000a] for the northeast Pacific with the high resolution Vancouver Island grid described by *Foreman et al.* [2004]. Model depths were computed by a smooth interpolation of data from the Canadian Hydrographic Service, *Smith and Sandwell* [1997], National Oceanic and Atmospheric Administration (NOAA) charts and GEODAS hydrographic survey data.

[1]Institute of Ocean Sciences, Fisheries and Oceans Canada, Sidney, British Columbia, Canada.
[2]Victoria, British Columbia, Canada.

0094-8276/08/2008GL035152$05.00

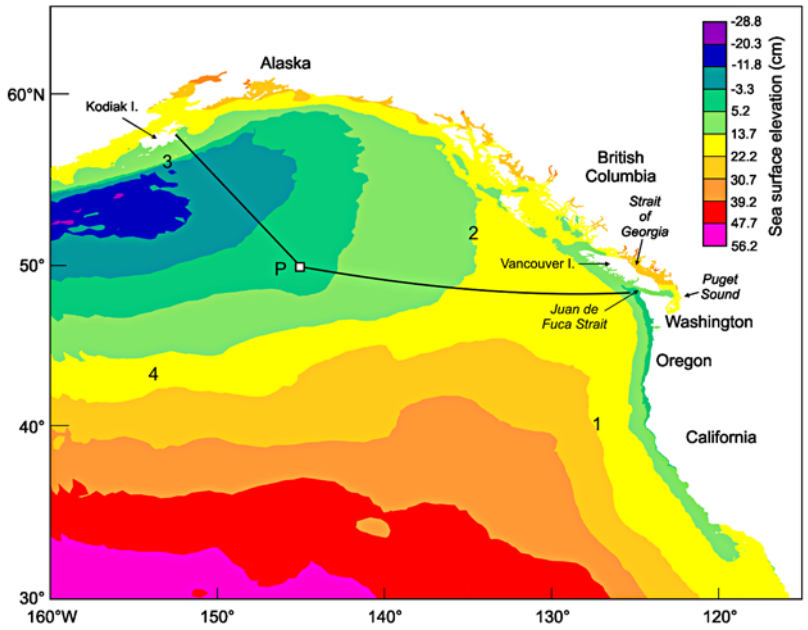

Figure 1. Average summer DOT (cm) computed from temperature and salinity climatology and NCEP wind stress. Consistent with TPJ seasonal averages, the elevation at Station P (white box) is adjusted to have the value 3.15 cm. Numbers mark the (1) California Current, (2) Alaska Current, (3) Alaskan Stream, (4) North Pacific Current, all flowing with higher sea levels on their right. Solid lines denote the transects used in Figure 3.

[6] As described by *Foreman et al.* [2000b], nonlinear bottom friction and vertical viscosity can be approximated in FUNDY5SP using root-mean-square (RMS) bottom and vertically averaged current speeds. In order that these RMS values include tides, our model was initially forced along the two open boundaries with harmonics for the eight tidal constituents M_2, S_2, N_2, K_2, K_1, O_1, P_1, and Q_1 taken from TPXO.6, an update of the Oregon State University global tidal model (http://www.coas.oregonstate.edu/research/po/research/tide/index.html), described by *Egbert et al.* [1994] and *Egbert and Erofeeva* [2002]. Off Vancouver Island, these eight constituents account for 86% of the tidal range. Tidal potential forcing, Earth tides, and ocean self-attraction and loading [*Ray*, 1998] were also applied as described in *Foreman et al.* [2000a]. The bottom friction and vertical viscosity coefficients were taken as 0.01 m s^{-1} and 0.1 m^2 s^{-1} respectively, and the solutions were computed iteratively to allow the RMS tidal values to converge.

[7] Average summer and winter wind stresses were computed from monthly mean NCEP (http://www.cdc.noaa.gov/cdc/data.ncep.reanalysis.derived.surface.html) re-analysis values. Consistent with *Boyer et al.* [2002] and *Stephens et al.* [2002], summer spanned July through September while winter spanned January through March. Seasonal temperature and salinity climatologies were computed from all available conductivity-temperature-depth (CTD), bottle, expendable bathy-thermograph (XBT), and Argo (http://www-argo.ucsd.edu/) data in NOAA, Marine Environmental Data Service (MEDS), and Institute of Ocean Sciences archives. Calculations were carried out in sixty-five subregions of the model domain and up to fifty-two level surfaces extending down to 5000 m. Seasonal averages were computed as the median of yearly seasonal values The resultant average temperature and salinity fields at the top forty-six depths for the northern portion of the model domain can be viewed at http://www-sci.pac.dfo-mpo.gc.ca/osap/data/alaska/default_e.htm.

3. Model Results and Comparisons With Satellite-Based Estimates

[8] In light of seasonal changes to the coastal winds and currents [*Freeland et al.*, 1984], average DOTs were computed for both summer and winter. Boundary conditions along the 30°N and 160°W edges of the model domain were a combination of geostrophic radiation conditions [*Lynch and Werner*, 1987] and specified elevations that permitted smooth inflow (outflow) to (from) the model interior. As the model elevations are only unique with respect to an arbitrary datum, the average summer elevations were shifted to have the same value of 0.0315 m at Station Papa (145°W, 50°N; see Figure 1) as the average summer anomaly interpolated from (inverse barometer and tidally corrected [*Cherniawsky et al.*, 2001]) TPJ elevations over the period of 23 September 1992 to 10 August 2002 (phase "A" of the TPJ mission). The winter elevations were shifted so that their value at Station Papa was -0.0504 m, also consistent with corresponding TPJ winter anomalies.

[9] The resultant DOT fields, as shown in Figures 1 and 2, are seen to be quite similar in the deep ocean. Both have a range of approximately 0.77m along 160°W with the highest values near 30°N and a depression just south of the Aleutian Islands. The overall pattern is consistent with the classical circulation picture [*Dodimead et al.*, 1963] of an eastward North Pacific Current that bifurcates into the California Current and Alaska Current. The latter current forms the eastern arc of the Alaskan Gyre that is centered over the low sea level region of the gulf. For comparison, the ranges along 160°W for the JPL DOT and the AVISO CMDT annual averages (not shown) are somewhat smaller

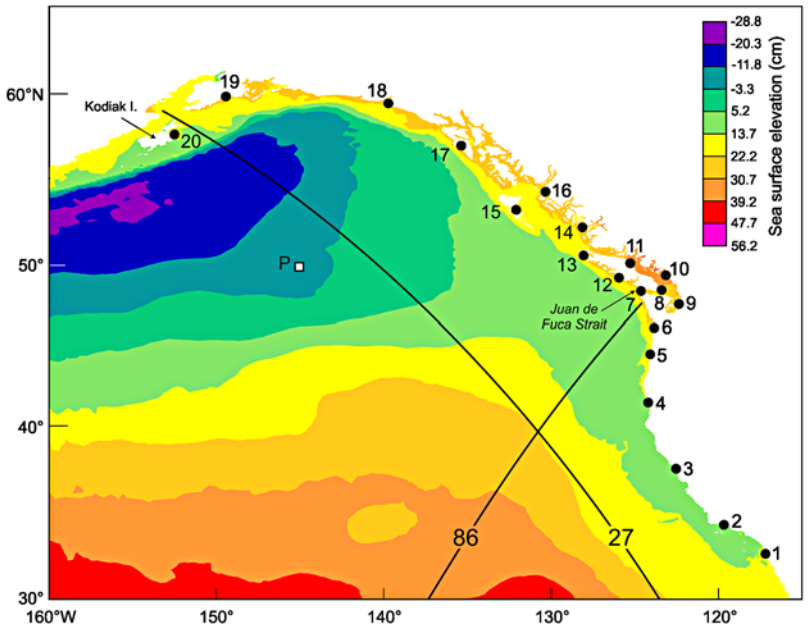

Figure 2. As in Figure 1 but for average winter DOT (cm) and the elevation at Station P (white box) is adjusted to have the value −5.04 cm. Numbered sites are tide gauges listed in Table 1. Solid lines denote the TPJ tracks used in Figure 4.

at approximately 0.66 and 0.63 m, respectively. The most likely reason for this disparity is that these JPL and AVISO images are only available on a 0.5° resolution grid and appear to have had significant smoothing. The DOT model fields (Figures 1 and 2) have significant seasonal differences along the California, Oregon, Washington, and British Columbia continental shelves where predominantly upwelling (downwelling) winds have produced a set-down (set-up) in the summer (winter) that is consistent with the elevations computed by *Foreman et al.* [1998] from five years of TPJ altimetry along the British Columbia shelf.

[10] Figure 3 illustrates these seasonal differences along two transects (see Figure 1) emanating from Station P. The first is along Line-P, while the second is along a line that extends roughly northward to Kodiak Island, Alaska. For comparison, the associated JPL DOT and AVISO CMDT values, shifted so that their elevations are zero at the model node closest to Station P, are also shown. Westward of their maxima at longitude 131°W in Figure 3a, the JPL and AVISO elevations lie approximately halfway between the model seasonal elevations. Eastward of this longitude, both the JPL and AVISO elevations slope down to the coast, while the model values continue upward to approximately 128°W, at which point they diverge, extending upward to the coast in winter and downward in summer.

[11] Figure 3b has a similar pattern. In this case, the JPL and AVISO elevations drop and are bracketed by the model values from Station P northward to their minima at about latitude 53.5°N, whereupon they slope upward toward the coast. On the other hand the two model elevations plateau between 53°N and 56°N before rising sharply at 56.6°N and then leveling off next to the coast of Kodiak Island. The much steeper model gradients are consistent with actual Alaskan Stream currents. Summer and winter geostrophic speeds of the Alaskan Stream are 44 and 34 cm s^{-1}, respectively, based on model slopes between 56.5°N and 56.9°N. These are much closer to maximum surface geo-

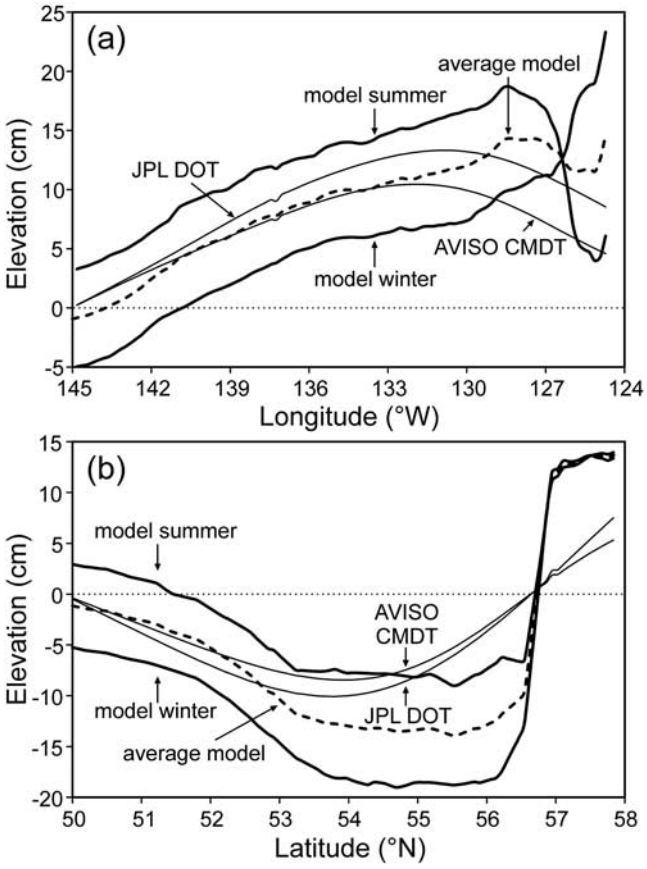

Figure 3. DOT (cm) along (a) Line P eastward from Station P to the entrance to Juan de Fuca Strait and (b) the transect that extends from Station P to Kodiak, Alaska (see Figure 1). The model, JPL DOT, and AVISO CMDT values have been adjusted so their annual means are zero at Station P. NB. Average model = average of summer and winter, only an approximation to the annual mean.

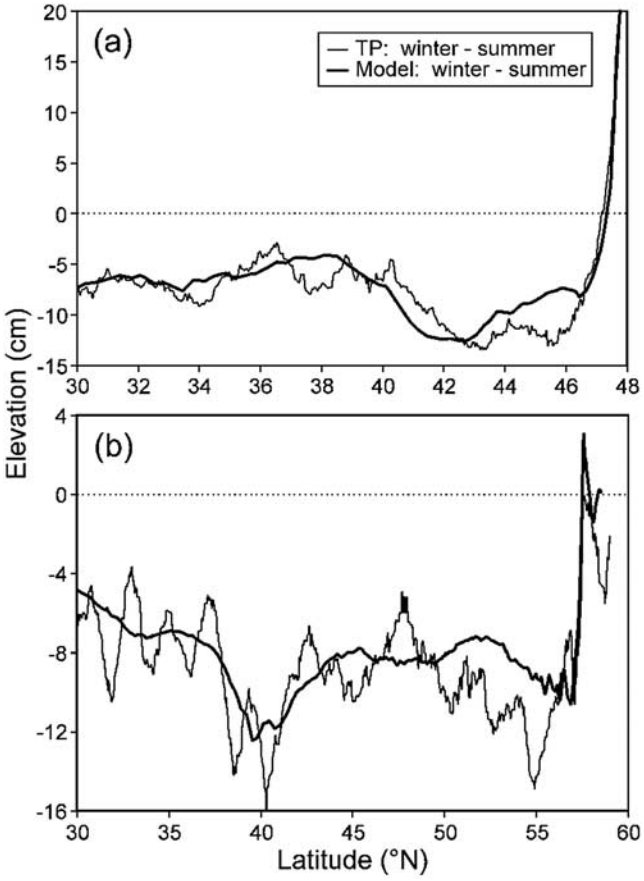

Figure 4. Average winter minus average summer elevations (in cm) along (a) TPJ track 86 and (b) TPJ track 27 (see Figure 2), compared to the corresponding differences in the model.

strophic currents of 65 cm s^{-1} between 155°W and 165°W reported by *Reed and Stabeno* [1999], and a factor of ten larger than speeds of 5.3 and 4.3 cm s^{-1} corresponding to JPL and AVISO slopes. Clearly, the JPL and AVISO ocean topography averages this narrow current over much too wide a region.

[12] Though only a reasonable approximation to the annual mean, an average of the summer and winter fields is also shown in Figure 3. As spring and fall are generally subject to more variability on the continental shelves, a careful examination of their temperature and salinity data will be carried out before computing and using those seasonal fields to produce a more accurate annual mean.

4. Comparisons With Satellite Altimetry and Coastal Tide Gauges

[13] Figure 4 compares winter minus summer elevation differences between the model and T/P satellite altimetry. (Given that the altimetry values are only available as anomalies until an accurate geoid is known, we cannot compare absolute elevations.) The first comparison (Figure 4a) is for track 86 which, within the model domain, extends northeastward from latitude 30°N and longitude 137°W to approximately 15 km off the Washington coast, just south of the entrance to Juan de Fuca Strait. Average and root mean square differences (model−altimeter) of 0.1 and 1.9 cm respectively demonstrate very good correspondence, particularly when the track moves onto the continental shelf and both elevation differences approach 20 cm.

[14] The second comparison (Figure 4b) is for track 27 which extends northwestward from latitude 30°N and longitude 127°W to the western portion of Cook Inlet. In this case, average and rms differences are again quite good, 0.9 and 2.2 cm respectively. Oscillations in the altimetric differences having an approximate amplitude of 3 cm and wavelength of 200 km most likely arise from migrating fronts and mesoscale eddies [*Crawford et al.*, 2002; *Ladd*, 2007] in the California Current, Alaskan Stream, and Gulf of Alaska.

[15] Table 1 compares model seasonal elevation differences with those computed at twenty coastal tide gauges (see Figure 2 for locations) whose averaging period was taken to be the same as for the altimetry. These data were downloaded from http://www.meds-sdmm.dfo-mpo.gc.ca/MEDS/Databases/TWL/TWL_e.htm and http://tidesonline.nos.noaa.gov/ and corrected for inverse barometer effects using NCEP average monthly atmospheric pressures. Despite the fact that several gauges are sited in harbors and thus subject to local effects that would not be captured by the model, the average and root mean square differences (model−gauge) of −0.7 and 3.7 cm respectively demonstrate reasonable agreement.

5. Summary and Discussion

[16] In this study, dynamic ocean topography for the northeast Pacific Ocean was computed independently of satellite observations by using a high resolution diagnostic model and seasonal climatologies of temperature, salinity, and wind stress. Values were shown to be in reasonable agreement with annually averaged JPL and AVISO estimates in the deep ocean but have poor agreement on continental shelves where these products lack data and are overly smoothed. The model estimates showed significant seasonal differences on continental margins and those differences were generally in good agreement with analogous values

Table 1. Tide Gauge and Model DOT Seasonal Differences[a]

Site	Site Number[b]	Tide Gauge	Model
San Diego	1	−5.8	−0.7
Santa Barbara	2	−3.6	−1.2
San Francisco	3	5.0	5.2
Crescent City	4	10.4	17.8
South Beach	5	19.3	22.4
Astoria	6	22.8	16.7
Neah Bay	7	18.5	16.5
Victoria	8	11.6	12.7
Seattle	9	13.7	9.3
Vancouver	10	9.4	5.7
Campbell River	11	9.6	10.2
Tofino	12	15.5	13.9
Winter Harbour	13	18.6	16.1
Bella Bella	14	13.4	8.3
QC City	15	3.5	2.6
Prince Rupert	16	11.4	5.8
Sitka	17	8.3	5.5
Yakutat	18	2.9	−0.7
Seward	19	−1.4	−2.3
Kodiak	20	−3.5	0.9

[a]Differences are given as winter minus summer (in cm).
[b]Site Number refers to the site location number shown on Figure 2.

computed from both satellite altimetry and coastal tide gauge measurements. This was despite the fact that the altimetry and tide gauge observations and the temperature/salinity/wind climatologies were not for exactly the same time period.

[17] Though the recently launched Jason-2 satellite will provide altimetry measurements closer to the coast than TPJ, present satellite-based gravity and altimetry observations are clearly not sufficient to compute DOT in nearshore regions. They need to be combined with either high resolution model calculations similar to those described above, or a relatively dense array of coastal and continental shelf tide gauge measurements of mean sea levels.

[18] The average seasonal and annual fields described above can be freely downloaded from http://www-sci.pac.dfo-mpo.gc.ca/osap/people/foreman_e.htm.

[19] **Acknowledgments.** We thank Trish Kimber for assistance with the figures; Brian Beckley and Richard Ray of Goddard Space Center for providing the TPJ altimeter data; one reviewer for his/her constructive comments; and the Canadian GEOIDE Networks of Centres of Excellence, and the Canadian Foundation for Climate and Atmospheric Studies Global Ocean-Atmosphere Prediction and Predictability Project for partial financial support.

References

Bingham, R. J., and K. Haines (2006), Mean dynamic topography: Intercomparisons and errors, *Philos. Trans. R. Soc., Ser. A*, *364*, 903–916.

Boyer, T. P., C. Stephens, J. I. Antonov, M. E. Conkright, R. A. Locarnini, T. D. O'Brien, and H. E. Garcia (2002), *World Ocean Atlas 2001*, vol. 2, *Salinity*, *NOAA Atlas NESDIS*, vol. 50, 165 pp., NOAA, Silver Spring, Md.

Cherniawsky, J. Y., M. G. G. Foreman, W. R. Crawford, and R. F. Henry (2001), Ocean tides from TOPEX/Poseidon sea level data, *J. Atmos. Oceanic Technol.*, *18*, 649–664.

Crawford, W. R., J. Y. Cherniawsky, M. G. G. Foreman, and J. F. R. Gower (2002), Formation of the Haida-1998 oceanic eddy, *J. Geophys. Res.*, *107*(C7), 3069, doi:10.1029/2001JC000876.

Dodimead, A. J., F. Favorite, and T. Hirano (1963), Salmon of the North Pacific Ocean: Part II. Review of oceanography of the subarctic Pacific region, *Bull. 13*, 195 pp., Int. North Pac. Fish. Comm., Vancouver, B. C., Canada.

Egbert, G. D., and S. Y. Erofeeva (2002), Efficient inverse modeling of barotropic ocean tides, *J. Atmos. Oceanic Technol.*, *19*, 183–204.

Egbert, G. D., A. F. Bennett, and M. G. G. Foreman (1994), TOPEX/POSEIDON tides estimated using a global inverse model, *J. Geophys. Res.*, *99*(C12), 24,821–24,852.

Foreman, M. G. G., W. R. Crawford, J. Y. Cherniawsky, J. F. R. Gower, L. Cuypers, and V. A. Ballantyne (1998), Tidal correction of TOPEX/POSEIDON altimetry for seasonal sea surface elevation and current determination off the Pacific coast of Canada, *J. Geophys. Res.*, *103*(C12), 27,979–27,998.

Foreman, M. G. G., W. R. Crawford, J. Y. Cherniawsky, R. F. Henry, and M. R. Tarbotton (2000a), A high-resolution assimilating tidal model for the northeast Pacific Ocean, *J. Geophys. Res.*, *105*(C12), 28,629–28,651.

Foreman, M. G. G., R. E. Thomson, and C. L. Smith (2000b), Seasonal current simulations for the western continental margin of Vancouver Island, *J. Geophys. Res.*, *105*(C8), 19,665–19,698.

Foreman, M. G. G., G. Sutherland, and P. F. Cummins (2004), M_2 tidal dissipation around Vancouver Island: An inverse approach, *Cont. Shelf Res.*, *24*(18), 2167–2185.

Freeland, H. J., W. R. Crawford, and R. E. Thomson (1984), Currents along the Pacific coast of Canada, *Atmos. Ocean*, *22*, 151–172.

Greenberg, D. A., F. E. Werner, and D. R. Lynch (1998), A diagnostic finite element ocean circulation model in spherical polar coordinates, *J. Atmos. Oceanic Technol.*, *15*, 942–958.

Henry, R. F., and R. A. Walters (1993), A geometrically-based, automatic generator for irregular triangular networks, *Commun. Numer. Methods Eng.*, *9*, 555–566.

Ladd, C. (2007), Interannual variability of the Gulf of Alaska eddy field, *Geophys. Res. Lett.*, *34*, L11605, doi:10.1029/2007GL029478.

Lynch, D. R., and F. E. Werner (1987), Three-dimensional hydrodynamics on finite elements. Part I: Linearized harmonic model, *Int. J. Numer. Methods Fluids*, *7*, 871–909.

Ray, R. D. (1998), Ocean self-attraction and loading in numerical tidal models, *Mar. Geod.*, *21*, 181–192.

Reed, R. K., and P. J. Stabeno (1999), A recent full-depth survey of the Alaskan stream, *J. Oceanogr.*, *55*, 79–85.

Rio, M.-H., and F. Hernandez (2004), A mean dynamic topography computed over the world ocean from altimetry, in situ measurements, and a geoid model, *J. Geophys. Res.*, *109*, C12032, doi:10.1029/2003JC002226.

Smith, W. H. F., and D. T. Sandwell (1997), Global sea floor topography from satellite altimetry and ship depth soundings, *Science*, *277*, 1956–1962.

Stephens, C., J. I. Antonov, T. P. Boyer, M. E. Conkright, R. A. Locarnini, T. D. O'Brien, and H. E. Garcia (2002), *World Ocean Atlas 2001*, vol. 1, *Temperature*, *NOAA Atlas NESDIS*, vol. 49, 167 pp., NOAA, Silver Spring, Md.

J. Y. Cherniawsky, W. R. Crawford, and M. G. G. Foreman, Institute of Ocean Sciences, Fisheries and Oceans Canada, P.O. Box 6000, Sidney, BC V8L 4B2, Canada. (mike.foreman@dfo-mpo.gc.ca)

J. Galbraith, 1920 Haultain Street, Victoria, BC V8R 2L5, Canada.